Journal of Nuclear Materials 390–391 (2009) 238–241

Contents lists available at ScienceDirect

Journal of Nuclear Materials

journal homepage: www.elsevier.com/locate/jnucmat

Highly radiating type-III ELMy H-mode with low plasma core pollution

J. Rapp [a,b,c,*], M.R. de Baar [a,b], W. Fundamenski [a,d], M. Brix [a,d], R. Felton [a,d], C. Giroud [a,d], A. Huber [a,c], S. Jachmich [a,e], E. Joffrin [a,f], I. Nunes [a,g], G.J. van Rooij [a,b], M. Stamp [a,d], G. Telesca [a,c], R. Zagorski [a,h], JET EFDA contributors [1]

[a] JET-EFDA, Culham Science Centre, OX14 3DB, Abingdon, UK
[b] FOM Instituut for Plasmfysica Rijnhuizen, Association EURATOM-FOM Nieuwegein, Trilateral Euregio Cluster, Postbus 1207, NL-3430 BE Nieuwegein, The Netherlands
[c] IEF-4, Forschungszentrum Jülich GmbH, Association Euratom-FZJ, Trilateral Euregio Cluster, Jülich, Germany
[d] EURATOM-UKAEA/Fusion Association, Culham Science Centre, Abingdon, OXON, UK
[e] Laboratory for Plasma Physics, ERM/KMS, Association EURATOM-Belgian State, Trilateral Euregio Cluster, Brussels, Belgium
[f] Association EURATOM-CEA sur la Fusion Controlee, Cadarache, Saint-Paul-lez-Durance, France
[g] Association EURATOM/IST, Centro de Fusao Nuclear, Lisbon, Portugal
[h] Institute of Plasma Physics and Laser Microfusion, EURATOM Assocation, Warsaw, Poland

ARTICLE INFO

PACS:
52.25.Vy
52.40.Hf
52.55.Fa
52.55.Rk

ABSTRACT

The impurity seeded type-III ELMy H-mode is proposed as an integrated ITER scenario. At JET this scenario has been demonstrated up to plasma currents of 3 MA with nitrogen as seeding gas. Detached divertor operation is achieved with significantly reduced steady state and transient heat fluxes. By operating in a high triangular magnetic configuration, very high central line-averaged electron densities are reached (up to 1.1×10^{20} m^{-3}). The impurity sources and impurity concentration in the plasma core were investigated for a broad range of plasma conditions in those highly radiating plasmas. The results are compared to an integrated model of the plasma edge and plasma core. On the basis of this modelling extrapolations to ITER are done with neon seeding, giving more confidence that these radiative plasmas will have a power amplification factor in excess of 10.

1. Introduction

One of the most severe problems for fusion reactors is the power load on the plasma facing components. Technically only loads of less than 10 MW/m^2 in steady state and less than 0.5 MJ/m^2 [1] during transients of 250 μs duration, caused by so-called Edge Localized Modes (ELMs), are acceptable. This effectively means that the unmitigated type-I ELMy H-mode is not acceptable for ITER. The challenge is to develop alternative scenarios, which combine sufficient energy confinement to achieve fusion power amplification factors of $Q = 10$, with benign heat loads to the plasma facing components.

The radiative type-III ELMy H-mode seems a possible solution for such an integrated ITER scenario. Most notably the transient heat loads due to type-III ELMs are acceptable with even the most stringent boundary conditions. For instance, on JET the transient energy loads due to type-III ELMs onto the outer divertor target were reduced to 2 kJ/m^2 [2] which corresponds to a ratio of divertor heat load to total stored energy of $\Delta W_{ELM}/W = 0.0003$, which is approximately 0.1% of the pedestal stored energy. The results on JET were achieved in experiments carried out with nitrogen seeding to mitigate the transient and steady state heat flux to the divertor. Significant radiative dissipation of the ELM energy was only observed at very small ELMs of ~10 kJ [2,3]. With the rough assumption that the ELM energy lost at the pedestal will increase by about a factor of 3, when lowering the pedestal collisionality to ITER values (JET #59029: $\nu^*_{ped,\|} \sim 0.55$; ITER 17MA: $\nu^*_{ped,\|} \sim 0.2$; see also [4,3]), the energy loss is expected to be $\Delta W_{ELM}/W_{ped} = 0.3\%$ for type-III ELMs in ITER. With a pedestal stored energy for type-III ELMy H-mode of about 110 MJ this would lead to a transient energy loss to the ITER divertor due to type-III ELM of approximately 0.3 MJ/m^2.

The drawback of the type-III ELMy H-mode is that the confinement is reduced by ~8–20% compared to the type-I ELMy H-mode base scenario. The reduction in stored energy could be regained by increasing the plasma current. Increasing the plasma current to $I_p = 17$ MA on ITER and hence reducing the edge safety factor to 2.6, would allow $Q = 10$ operation at a confinement enhancement factor of $98_{(y,2)} = 0.75$. This operation scenario was demonstrated at JET, with most normalized parameters within the ITER operation

* Corresponding author. Address: FOM Instituut for Plasmfysica Rijnhuizen, Association EURATOM-FOM Nieuwegein, Trilateral Euregio Cluster, Postbus 1207, NL-3430 BE Nieuwegein, The Netherlands. Tel.: +31 30 6096828; fax: +31 30 6031204.
E-mail address: J.Rapp@rijnhuizen.nl (J. Rapp).

[1] See the Appendix of M.L. Watkins et al., Fusion Energy 2006 (Proc. 21st Int. Conf. Chengdu, 2006) IAEA, 2006.

0022-3115/$ - see front matter © 2009 J. Rapp. Published by Elsevier B.V. All rights reserved.
doi:10.1016/j.jnucmat.2009.01.066

domain [4]. However, the effective plasma charge (Z_{eff} = 2.2) was marginally outside the operation range and needed improvement.

2. Experiments at high density

In the last JET campaigns (2006, 2007) the operation domain of this strongly radiating type-III ELMy H-mode was extended to higher plasma current (3 MA) and hence higher densities. Higher confinement was reached ($98_{(y,2)} = 0.83$) by optimized fuelling. The fuelling rate in those discharges is $\Gamma_D \sim 8 \times 10^{22}\,s^{-1}$ and $\Gamma_{N2} \sim 0.4\text{–}1.5 \times 10^{22}\,s^{-1}$. Electron densities of up to $1.1 \times 10^{20}\,m^{-3}$ were reached (normalized to the Greenwald $N^{GW} = n_e/n^{GW} = 1$) in high triangularity pulses. At those high densities the Z_{eff} was reduced below 1.4 as the data for the high-δ pulses show in Fig. 1. Fig. 1 illustrates that the Z_{eff} for the high triangularity pulses at high density is decreasing stronger than the simple scaling $Z_{eff} - 1 \propto P_{rad}/n_e^2$ suggests. To investigate this behaviour further, a heating power scan was performed in which the normalized beta β_N was increased from 1.5 to 1.9. During this heating power scan the radiative power fraction of 70% was kept constant by radiation feedback control acting on the nitrogen gas injection. Simultaneously the electron density was kept the same at about $1 \times 10^{20}\,m^{-3}$ by constant deuterium fuelling. The deuterium was fuelled in the private flux region of the inner divertor, while nitrogen was injected in the private flux region and the Scrape-Off Layer (SOL) in the outer divertor. The divertor is pumped in the inner private flux region and the outer SOL. By this scan P_{rad} was increased from 10.7 MW to 16.8 MA approximately. This resulted in an increase of the nitrogen fluxes of about a factor 4 in the divertor and on the main chamber walls, when going from a β_N of 1.5 to 1.9. In this scan the Z_{eff} was varied between 1.4 and 2. In Fig. 2 nitrogen fluxes at the edge, Z_{eff} and P_{rad} are shown versus the nitrogen plasma core concentration, as derived from charge exchange recombination spectroscopy (CXRS).

Z_{eff} as well as P_{rad} are linear increasing with the nitrogen core concentration and nitrogen fluxes at edge as expected, and $(Z_{eff} - 1)$ is proportional to P_{rad}. The linear increase of Z_{eff} with the nitrogen concentration suggests that the carbon concentration is not changing with increasing nitrogen fuelling and remains constant at a level of approximately 1%, while the nitrogen concentration is increased to almost 2% dominating the plasma conditions. The fact that the carbon level is unchanged is surprising since

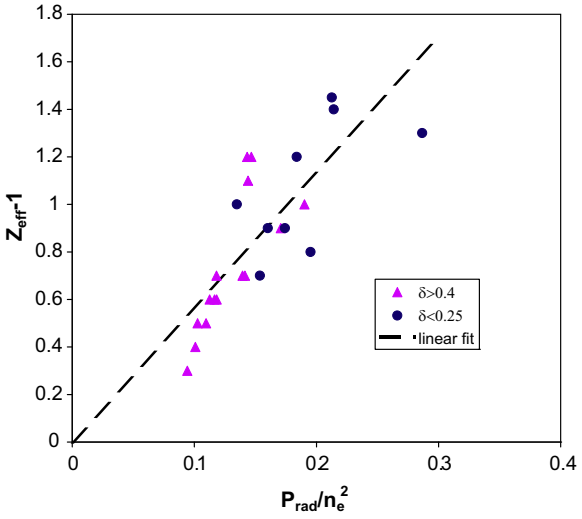

Fig. 1. $Z_{eff} - 1$ versus the empirical scaling P_{rad}/n_e^2 for nitrogen seeded type-III ELMy H-modes for high and low triangluarity pulses.

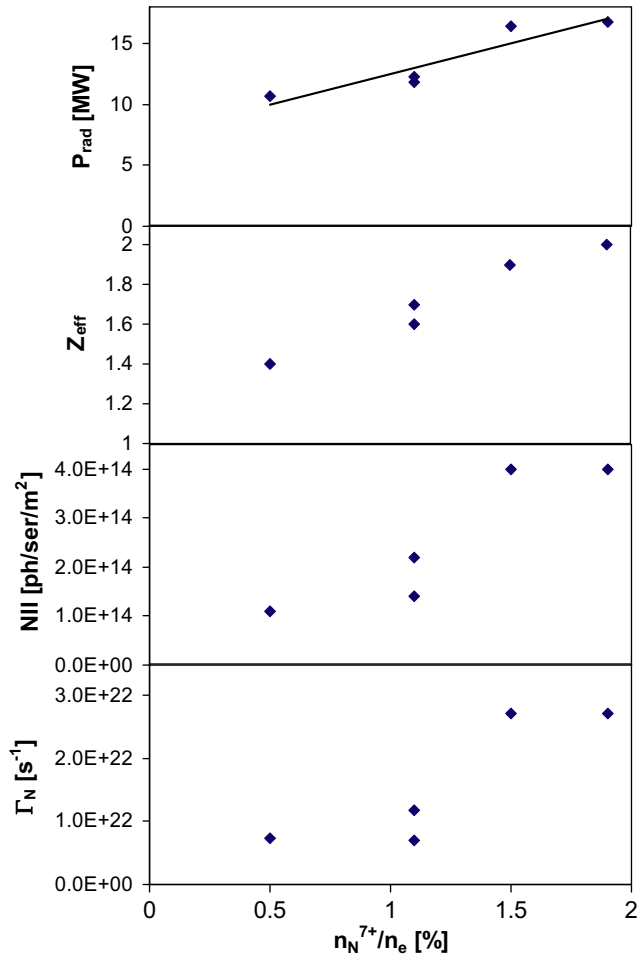

Fig. 2. Heating power scan with fixed radiative power fraction (70%) and fixed electron density ($1 \times 10^{20}\,m^{-3}$); (a) P_{rad} versus nitrogen core concentration; (b) Z_{eff} versus nitrogen core concentration; (c) NII versus nitrogen core concentration; (d) nitrogen influx versus nitrogen core concentration.

one would expect an increase of carbon release by physical sputtering since the nitrogen fluxes onto the plasma wall components are increased by a factor of 4. From the nitrogen fluxes into the plasma and the nitrogen concentration in the core also the fuelling efficiency can be calculated $S = \Delta N_N/(\Gamma_N \tau_p^*)$ [5]. With the assumption of $\tau_E = \tau_p^*$ a fuelling efficiency of S = 0.018 has been evaluated for the fuelling efficiency of nitrogen from the outer divertor. It should be noted that nitrogen is a non-recycling impurity and should behave approximately like carbon. For some good measurements (modest change of plasma background during nitrogen puff) τ_p^* was found to be up to a factor of 1.6 higher than τ_E, meaning that the fuelling efficiency could be about S = 0.01.

In the following the carbon sources in those highly radiating discharges are examined. The divertor carbon source is derived from the CIII line emission at 465 nm and the approximation $\Gamma_C = 5 \times 10^6\ (I^I + I^O)$ for the divertor fluxes, where I^I and I^O are the carbon CIII light in the inner and outer divertor [5]. With reduced power to the target the divertor carbon fluxes are reduced (Fig. 3) and behave similar to data of a small subset of low triangularity pulses [4]. However, for the high current (2.75 MA and 3 MA), high density discharges the divertor carbon source only varies by 20%, as indicated by the triangles in Fig. 3. Fig. 4 shows a comparison of the carbon source from the divertor to the main chamber wall. Similar to the divertor carbon sources, the main chamber carbon sources depend neither on power nor on the nitrogen fluxes into the SOL.

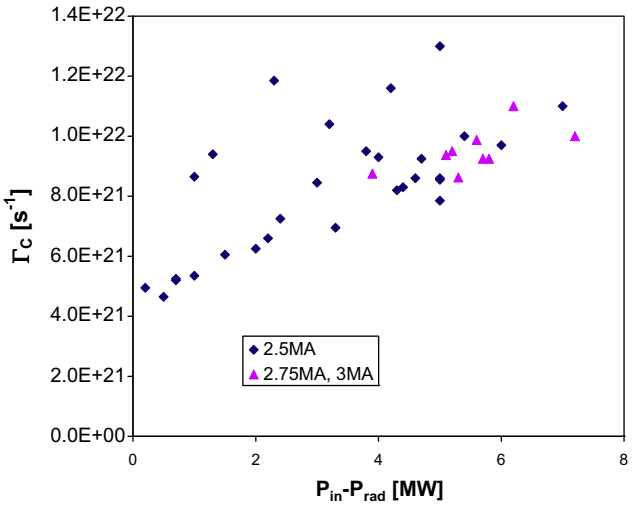

Fig. 3. Carbon divertor flux versus power to the divertor target. The data include the pulses shown in Fig. 2 (triangles). P_{in} is varies between 8 and 24 MW.

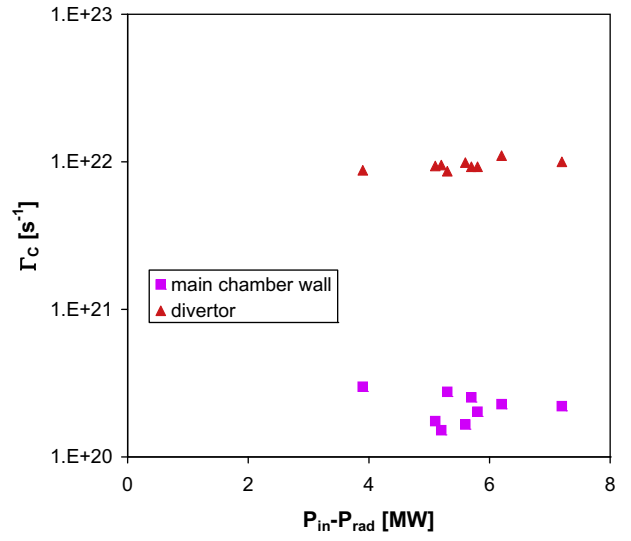

Fig. 4. Carbon divertor and main chamber flux versus power to the divertor target.

Fig. 5 indicates that the chemical erosion does increase slightly. The increase of the chemical erosion could be due to the higher target surface temperatures at the higher power fluxes to the target. In those discharges the surface temperature is always below the maximum temperature of the chemical erosion yield of 600 K [6,7]. However, the surface target temperature depends also on the discharge history and hence could also explain the scatter in the chemical erosion yield. The deuteron particle flux does not increase in this scan. This suggests, that the physical sputtering must be the minor release mechanism and that the chemical erosion determines the carbon erosion in those high density highly radiating detached divertor conditions. For details of divertor detachment see Ref. [2].

Fig. 4 also demonstrates that the carbon source in the divertor is about a factor of 50 larger than the carbon source in the main chamber. However the impurity screening is higher in the divertor than from the main chamber wall [5,8]. In comparison to the type-I ELMy H-mode the carbon source in the main chamber is lower for the type-III ELMy H-mode. This is consistent with observations that the transient heat loads due to type-III ELMs are deposited completely in the divertor, while for the type-I ELMy H-mode part

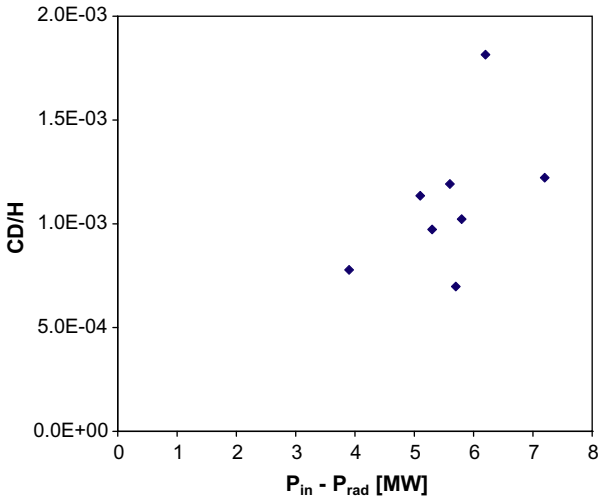

Fig. 5. CD/H_α versus power to the target.

of the ELM energy is deposited on main chamber components. This, as a consequence, leads to a lower fuel retention in the type-III ELMy H-mode, when compared to the type-I ELMy H-mode [9].

Taking a fuelling efficiency from the divertor of approximately 0.02, together with a carbon source in the divertor of $\Gamma_C = 1 \times 10^{22}\ s^{-1}$ would lead to carbon core concentrations of about 0.7%, which translates into a base Z_{eff} of 1.2. This is consistent with the Z_{eff} without the contribution from nitrogen as observed in Fig. 2.

3. Extrapolation to ITER

The new results of those high density radiating type-III ELMy H-modes have been added to a database of other nitrogen seeded type-III ELMy H-modes, including data from the former Mk-I, Mk-II, Mk-IIGB and Mk-SRP divertors. The Z_{eff} data from the new high density discharges extended the database to the lower end of the Z_{eff} scaling. In addition the scaling was re-evaluated taking into account the radial transport of the impurity ions. As already shown for radiative discharges on TEXTOR the radiation efficiency depends on the radial transport [10].

$$P_{rad} \propto C_z n_e^2 L_z(T_e, \tau_p^*),$$

with L_z being the cooling rate for the impurity in the coronal equilibrium modified for radial transport. This means that in the presence of transport the impurities can radiate at higher temperatures than in coronal equilibrium. In addition we assume the ionization time of the impurity to be $\tau_{ion}^Z \propto 1/n_e$ and can re-write the radiative power as $P_{rad} \propto C_z n_e^{3/2} L_z \sqrt{D_\perp}$ as described in more detail in [11]. At the plasma edge of a divertor tokamak we can re-write $\sqrt{D_\perp} \propto \sqrt{\tau_\parallel}/\tau_p$ according to [12]. Furthermore we assume that the effective particle confinement time is approximately close to the global energy confinement time $\tau_p^* = \tau_E$. Including those modifications, the scaling law is described as

$$Z_{eff} = 1 + 40 P_{rad} Z^{0.12} \tau_E S^{-0.94} n_e^{-1.5} a_{min}^{-1} R^{-1},$$

and yields a good fit to the experimental data (see Fig. 6). It should be noted that the regression with respect to the impurity charge Z and plasma surface S has not been changed and is kept as a result of the previous multi-machine and multi-species regression [13]. On the basis of this scaling the Z_{eff} for ITER can be estimated. For the high density 17 MA scenario with a fusion power of 400 MW and a $98_{(y,2)} = 0.75$ a Z_{eff} of 1.9 is predicted, excluding any contribution from Helium. This is a little above the assumptions made for

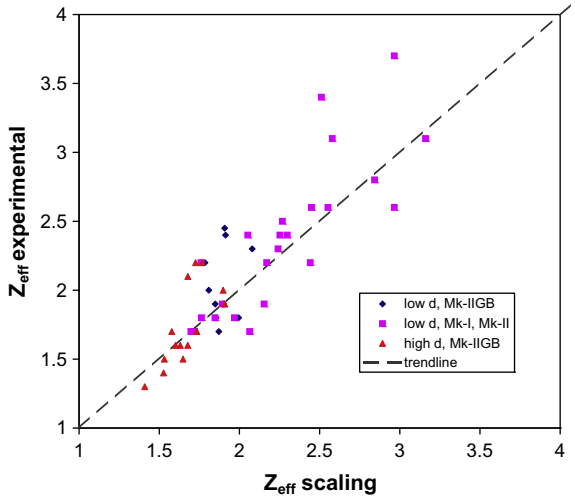

Fig. 6. Experimental Z_{eff} versus new Z_{eff}-scaling.

ITER, which include Helium. However, details of the radial impurity transport and profile effects in the temperature and density profiles are not taken into account. For example experimentally it is often found that the Z_{eff} profile is hollow [13].

Therefore a comparison with an integrated model [14] has been done. This integrated model, COREDIV, has been benchmarked to the nitrogen seeded JET discharges at high current [15]. The integrated model was able to match the experimental cases quite well.

On the basis of this benchmarking simulations for ITER have been done for neon seeding [15]. In all cases the carbon erosion from the divertor is strongly reduced, leading to a diminishing carbon core concentration. Neon is the dominating core impurity leading to Z_{eff} of approximately 1.5. However, the model cannot predict the Be erosion in the main chamber appropriately, which leads to an underestimation of the Z_{eff}.

4. Conclusions

The operation domain of the highly radiating type-III ELMy H-mode has been extended to higher densities and hence lower plasma core pollution. The main impurity in those discharges is the seeded element nitrogen. Carbon remains at a level of approximately 0.7% in the plasma core. The carbon sources seem to be independent of the nitrogen content and fluxes at the edge at those high densities, suggesting that physical sputtering is minimal and chemical erosion is dominating the carbon fluxes in those at least partially detached plasmas with type-III ELM edge. In those discharges nitrogen is the dominating impurity, replacing carbon as a radiator. This also leads to the suggestion that with nitrogen seeding a radiating detached divertor can be achieved with high-Z metal divertor targets.

Acknowledgement

This work was conducted under EFDA and partially funded by EURATOM.

References

[1] W. Fundamenski, J. Nucl. Mater. 390–391 (2009) 696.
[2] J. Rapp et al., Plasma Phys. Control. Fusion 44 (2002) 639.
[3] J. Rapp et al., Nucl. Fusion 44 (2004) 312.
[4] J. Rapp et al., J. Nucl. Mater. 337–339 (2005) 826.
[5] J. Strachan et al., Nucl. Fusion 43 (2003) 922.
[6] V. Philipps et al., Plasma Phys. Control. Fusion 42 (2000) B293.
[7] J. Roth, J. Nucl. Mater. 266–269 (1999) 51.
[8] J. Strachan et al., J. Nucl. Mater. 390–391 (2009) 92.
[9] T. Loarer et al., J. Nucl. Mater. 390–391 (2009) 20.
[10] G. Telesca et al., Nucl. Fusion 40 (2000) 1845.
[11] M.Z. Tokar, Nucl. Fusion 34 (1994) 853.
[12] G. Fussmann, Nucl. Fusion 26 (1986) 983.
[13] G.F. Matthews et al., Nucl. Fusion 39 (1999) 19.
[14] R. Zagorski, R. Stankiewicz, J. Nucl. Mater. 313–316 (2003) 899.
[15] R. Zagorski et al., Contrib. Plasm. Phys. (2008).